

Assessment of impact velocity effects on damage in armor materials through experimental and FEM analysis

Osman İyibilgin^{1,*}, Abdullah Mimaroglu¹

¹ Department of Mechanical Engineering, Sakarya University, 54050 Sakarya, Turkey

*Corresponding author E-mail: iyibilgin@sakarya.edu.tr

ABSTRACT

In this study, the deformation behavior of armor (plate) systems composed of high-strength ballistic steels MARS 190 and MARS 240 arranged in various thicknesses and combinations was investigated under different projectile impact velocities and angles using both experimental methods and the finite element method (FEM). In the experimental stage, four different plate configurations were prepared: single steel plate, double steel plates, steel–rubber–steel, and steel–air gap–steel combinations. These configurations were subjected to ballistic impacts at varying velocities. For each configuration, the level of deformation, energy absorption capacity, and structural integrity were analyzed.

The same test scenarios were modeled numerically using FEM, and the simulation results were validated through comparison with the experimental findings. Upon validating the analysis model, the number of composite plate models was increased. The results highlight the influence of impact velocity and plate composition on deformation behavior, revealing that multilayered and gapped structures effectively optimize energy distribution. The performance of different combinations of MARS 190 and MARS 240 materials was comparatively evaluated, and recommendations for effective armor design were provided. This study aims to contribute to engineering applications concerning the design of ballistic protection systems and material selection.

Keywords: LS-Dyna, finite element method (FEM), projectile velocity, composite armor, impact angle.

1. Introduction

With the increasing prevalence of ballistic threats in modern times, the development of armor systems has become critically important. In this context, high-strength armor steels such as MARS 190 and MARS 240 stand out due to their superior hardness and energy absorption capabilities. Studies aimed at determining their mechanical properties under dynamic loading have reported that the mechanical performance of these steels is significantly influenced by high strain rates [1], [2].

In the literature, the effects of multilayer and hybrid armor configurations on impact energy distribution and deformation mechanisms have been thoroughly examined. In particular, flexible interlayer structures such as steel–rubber–steel have been shown to mitigate stress waves, thereby assisting in balancing the structural load [3], [4]. Additionally, spaced armor systems have been reported to provide advantages in reducing the intensity of ballistic energy and are widely utilized in military vehicles [5].

In this study, the ballistic performance of MARS 190 and MARS 240 materials was investigated across four different armor configurations: single-layer, double-layer, steel–rubber–steel, and steel–air gap–steel. During the experimental stage, tests were conducted at various velocities (800, 1000, 1500 m/s) and impact angles (0°, 15°, 30°) to analyze the deformation levels, energy absorption capacities, and structural integrity of each configuration. The findings were validated through finite element simulations using ANSYS, aligning well with the existing literature [6].

The results clearly demonstrate the influence of both impact velocity and armor composition on deformation behavior. Notably, multilayered and spaced structures enhance durability by distributing energy more

effectively [7]. These findings aim to contribute significantly to engineering applications by informing material and structural selection in armor design.

2. Material and method

In this study, both experimental and numerical methods were employed to obtain data, which were then compared and interpreted.

2.1. Material

The armor steels used in this study are MARS 190 and MARS 240, which are well known for their high hardness, impact resistance, and energy absorption capacity. These steels possess distinct microstructural characteristics and mechanical properties, and are widely utilized in ballistic applications [4]. While MARS 190 exhibits a more ductile behavior, MARS 240 stands out with its higher hardness values [8]. In this study, structures with a thickness of 5 mm were used to create various combinations. In some configurations, a 5 mm thick rubber layer was inserted between two steel plates, or an air gap was introduced to form spaced structures. Table 1 presents the chemical compositions and mechanical properties of MARS 190 and MARS 240 steels.

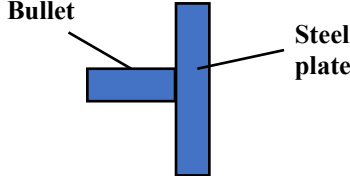
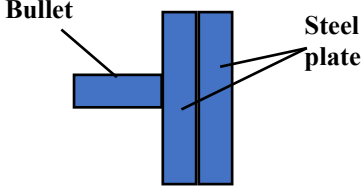
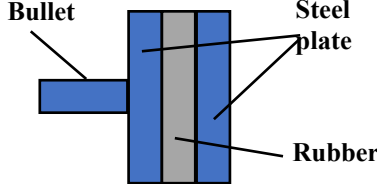
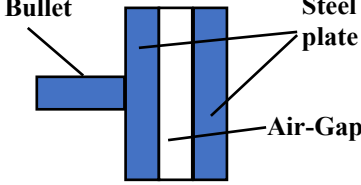
Table 1. Maximum chemical composition values and mechanical properties of MARS 190 and MARS 240 armor steels

MARS 190								
C	S	P	Si	Mn	Ni	Cr	Mo	V
0.3	0.005	0.012	0.4	1.2	2.0	1.0	0.6	0.1
Hardness (HB)		Yield Strength (MPa)		Tensile Strength (MPa)		Elongation at Break (%)		Notch Impact at - 40 °C (J/cm)
332/338		850		1100		12		25
331/375		830		1060		12		30
302/341		750		970		12		40
262/331		650		850		14		45
248/285		600		800		14		70
212/248		500		680		14		80
MARS 240								
C	S	P	Si	Mn	Ni	Cr	Mo	V
0.3	0.005	0.012	0.4	1.2	2.0	1.0	0.6	0.1
Hardness (HB)		Yield Strength Re 0.2% (MPa)		Tensile Strength Rm (MPa)		Elongation at Break A(5d) (%)		Notch Impact at - 40 °C (J/cm)
477/534		≥1100		≥1600		≥9		≥20

2.2. Plate combination

In the experimental study, four different armor configurations were investigated. These combinations are presented in Table 2.

Table 2. Armor configurations used in the study (each layer is 5 mm thick)

Combination Number	Plate Combination	Description
1		Single-piece steel plate
2		Two-piece steel plate
3		Three-piece composite plate
4		Three-piece composite plate

The literature also highlights that multilayered armor systems are more effective in terms of energy dissipation and deformation control [9], [4], [10]. Furthermore, the hardness of the armor material plays a crucial role in determining its mechanical resistance [11].

2.3. Experimental method

Ballistic tests were conducted using a specialized test setup, as shown in Figure 1, where each configuration was subjected to firing from a G3 rifle with a muzzle velocity of 800 m/s. This experimental work was carried out to validate the finite element analyses. The tests employed 7.62 mm caliber ammunition. To assess the deformation resulting from the impact, the specimens were carefully sectioned around the damaged area and measured using a caliper with a precision of 0.05 mm. It was observed that the deformation on the plate increased with the rise in projectile impact velocity. The obtained results were found to be consistent with previous literature [2].

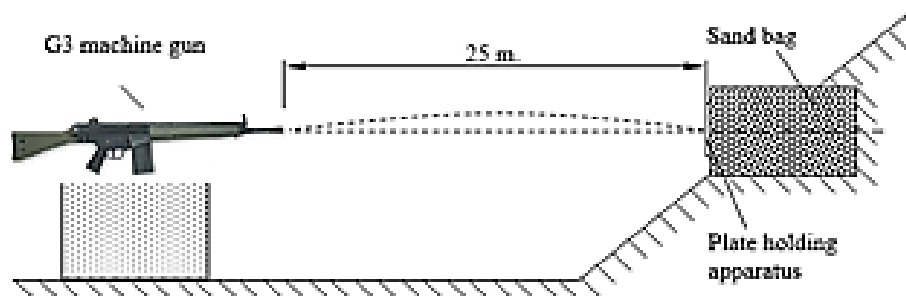


Figure 1. Experimental test setup [4]

2.4. Numerical method (finite element analysis)

Simulations were performed using ANSYS software and modeled to closely replicate the experimental test scenarios. The high-velocity impact behavior of MARS 190 and MARS 240 steels was characterized using the Johnson–Cook yield model [12], [13]. Three-dimensional solid elements (Solid 164) were selected as the element type. Such models are widely employed in high-precision impact analyses [14], [15], [16], [17].

In this study, the mechanical responses resulting from the impact of a high-speed projectile on the target armor plate were analyzed via the finite element method. During the modeling process, the initial contact of the projectile with the target represents the stage where compressive stresses predominantly develop on the plate surface. As the projectile penetrates the target material, tensile stresses arise on the lateral surfaces of the plate, causing bulging (bulge formation) on the rear face of the plate.

When the stress values exceed a certain threshold, full penetration of the target plate occurs, accompanied by physical damage characterized by material spalling. Under threshold stress levels, only partial penetration is observed. During numerical modeling, the target plate was meshed with sufficient refinement to capture detailed behaviors. Elements exceeding the specified stress limit were removed from the model in accordance with the damage criterion [2]. This approach effectively monitored the deformations and material loss occurring in the armor plate.

3. Results and discussion

In this study, the ballistic performance of different armor configurations composed of MARS 190 and MARS 240 armor steels against ballistic impacts was investigated using both experimental and numerical methods. The obtained results clearly demonstrated the effects of impact velocity and armor structure on deformation behavior and energy absorption capacity.

The analyses were conducted as transient and nonlinear simulations. Within this framework, time-dependent forces and displacements during the projectile penetration into the target were calculated. The analysis results enabled the determination of the projectile's residual velocity after perforation and the bulge size formed on the rear side of the plate [18]. These parameters are directly related to the armor material's energy absorption capacity and play a critical role in armor design [19].

3.1. Deformation behavior

Experimental tests revealed that in single-layer armor structures, deformation spread over a wider area and localized indentations occurred in the impact zone. Due to its higher hardness, MARS 240 steel exhibited greater resistance at the initial impact; however, it demonstrated brittle behavior under high-velocity impacts. In contrast, MARS 190 steel showed more ductile deformation and a lower tendency for fragmentation after impact. In the experimental study, tests were conducted using G3 ammunition with an impact velocity of 800 m/s, and the results were compared to validate the analytical model. Finite element analyses also examined plate combinations not included in the experimental work, and the obtained results were discussed.

Figure 2 presents the projectile velocity–time graph resulting from the impact of a projectile traveling at 1000 m/s on plates with thicknesses of 10, 15, and 20 mm. Analysis of the graph indicates partial deformation for the 15 mm and 20 mm thick plates, whereas the 10 mm thick plate experienced complete penetration.

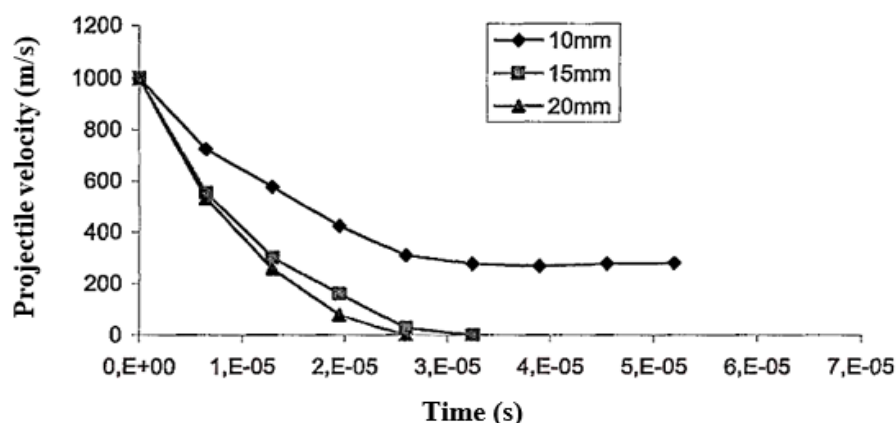


Figure 2. Time-dependent projectile velocity at 1000 m/s impact velocity (0° impact angle)

Figure 3 illustrates the velocity–time graph of a projectile fired at 1000 m/s impacting composite plates with a thickness of 15 mm in different configurations. Examination of the figure reveals that partial damage occurred in all configurations, but complete perforation of the plate was not observed. While the 10 mm thick plate shown in Figure 2 experienced full penetration, it was observed that when a 5 mm air gap was introduced between two 5 mm thick plates, as depicted in Figure 3, the plate was not fully penetrated.

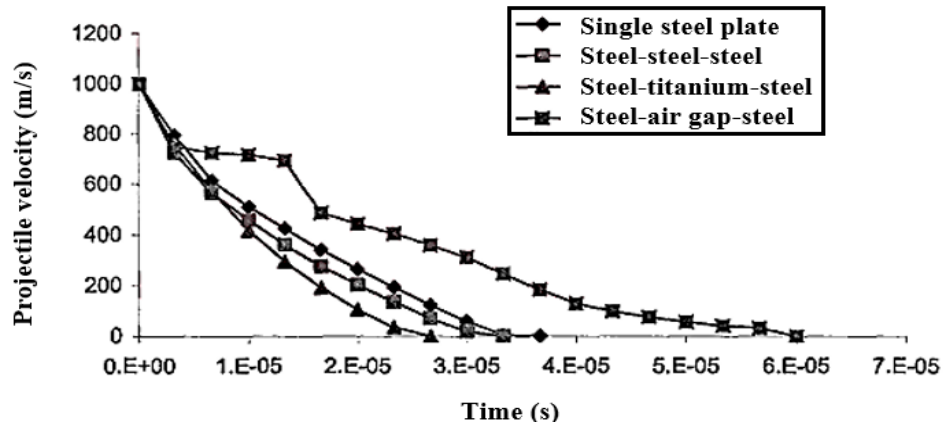


Figure 3. Time-dependent projectile velocity for target plates with four distinct composite configurations, each with a total thickness of 15 mm, under an impact velocity of 1000 m/s

Table 3. Summary of damage conditions depending on armor thickness, projectile impact angle, and projectile velocity

Steel plate thickness (mm)	Projectile Impact Angle (Degree)	Projectile velocity (m/s)	Bulging on the Back Face of the Plate (mm)	Projectile Residual Velocity After Penetration (m/s)
10	0°	800	7.45	not penetrated
		1000	6.59	92
		1500	1.55	881
	15°	800	9.82	not penetrated
		1000	6.43	39
		1500	5.5	786
	30°	800	6.57	not penetrated
		1000	11	not penetrated
		1500	5.15	795
15	0°	800	3.9	not penetrated
		1000	5.61	not penetrated
		1500	3.56	428
	15°	800	6.09	not penetrated
		1000	9.51	not penetrated
		1500	4.48	640
	30°	800	2.75	not penetrated
		1000	5.37	not penetrated
		1500	7.54	not penetrated
20	0°	800	2.37	not penetrated
		1000	3.39	not penetrated
		1500	6.29	not penetrated
	15°	800	1.44	not penetrated
		1000	1.77	not penetrated
		1500	3.6	not penetrated
	30°	800	1.36	not penetrated
		1000	2.08	not penetrated
		1500	3.49	not penetrated

Table 3 summarizes the damage states obtained as a function of armor thickness, projectile impact angle, and projectile velocity. This demonstrates that material selection depends not only on hardness values but also on the plastic deformation capacity under impact loading [20], [3].

Penetration of the armor is an undesirable event, as the resulting damage can be fatal. In cases where the armor is not penetrated, the bulging damage on the rear side helps to assess the extent of the impact.

Based on the data presented in Table 3, it was concluded that an impact velocity of 1000 m/s and a projectile impact angle of 0° (normal incidence) represent critical conditions. Under these circumstances, composite structures were designed and analyzed. Table 4 presents the analysis results for three different composite configurations subjected to a projectile velocity of 1000 m/s and an impact angle of 0° (normal incidence).

Table 4. Composite plate combinations with a total thickness of 15 mm.

Steel plate thickness (mm)	Projectile Impact Angle ($^\circ$)	Projectile velocity (m/s)	Bulging on the Back Face of the Plate (mm)	Projectile Residual Velocity After Penetration (m/s)
S-S-S Steel-Steel-Steel 5-5-5	0°	1000	7.54	0
S-T-S Steel-Titanium-Steel 5-5-5	0°	1000	6.54	0
S-A-S Steel-Air gap-Steel 5-5-5	0°	1000	12.5	0

An examination of Table 4 reveals that the armor combination containing titanium undergoes less deformation. The second highest bulging is observed in the model consisting of three steel plates arranged consecutively, which exhibits approximately 13% more bulging compared to the titanium-containing model. When an air gap is introduced, the bulge increases by 47%. Although none of the three composite structures experienced perforation, the composite structure with the air gap offers a 33% reduction in both cost and weight. Therefore, despite the increased bulging in the armor plate, the reduction in cost and weight enhances mobility and provides more sustainable solutions.

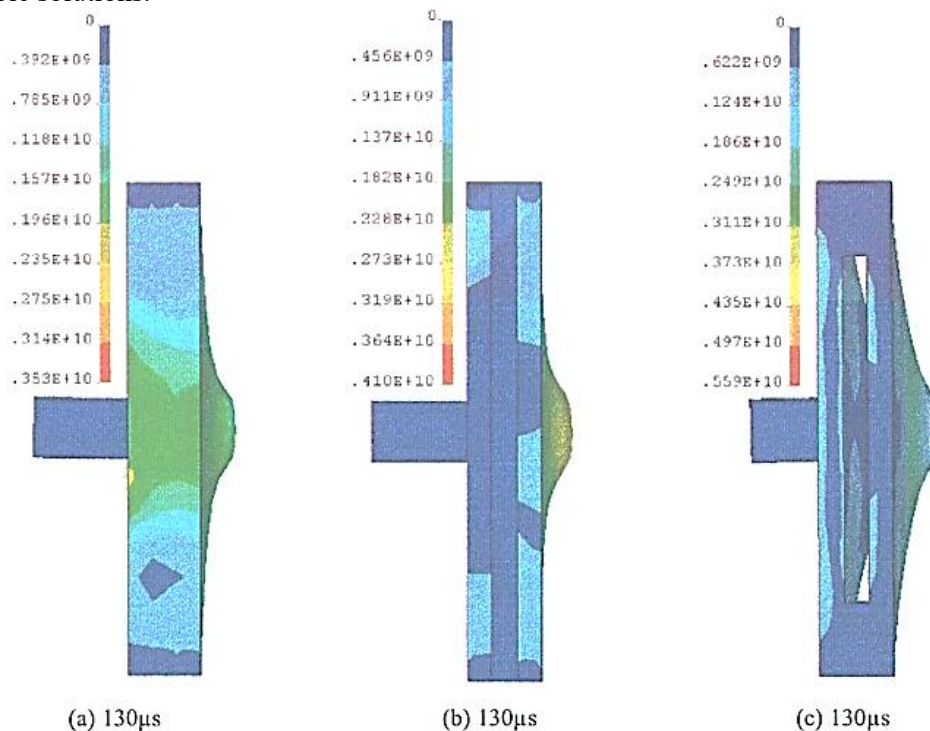


Figure 4. Deformation patterns on the target at an impact velocity of 1000 m/s: a) S-S-S, b) S-T-S, c) S-A-S (NB: S = Steel, T = Titanium, A = Air gap)

Figure 4 illustrates the damage patterns formed when a cylindrical projectile traveling at 1000 m/s impacts the target plate with a total thickness of 15 mm. As shown in Figure 3, the bulge values on the target plate vary depending on the armor configuration. The STS (Steel-Titanium-Steel) combination results in the lowest bulge value. However, despite exhibiting greater bulging, the SAS (Steel-Air gap-Steel) model is more efficient in terms of weight and cost. No penetration occurred at an impact velocity of 1000 m/s, and the SAS model demonstrated more sustainable performance.

3.2. Impact of layered armor structures

Two-layered structures preserved structural integrity more effectively after impact by distributing deformation more evenly compared to single plates. In particular, the steel–rubber–steel configuration exhibited the highest energy absorption capacity due to the elastomeric interlayer damping the stress waves. This structure reduced rear-face deformation after impact and prevented perforation of the plate [9], [6]. The steel–air gap–steel configuration also significantly reduced the transmitted impact energy to the second layer by dissipating most of the force in the first layer. Additionally, after perforating the first layer, the projectile's trajectory was deflected, further diminishing the deformation effect [5], [21].

At an impact velocity of 800 m/s, no penetration occurred in the 10 mm thick plate. However, at 1000 m/s, penetration behavior varied depending on plate thickness: the 10 mm plate was fully penetrated, the 15 mm plate experienced partial penetration, and no penetration was observed in the 20 mm plate [12]. Therefore, composite armor configurations were analyzed under the condition of 15 mm total thickness and 1000 m/s projectile velocity.

Figure 5 presents a graph showing the exit velocity of the projectile after penetrating the target, depending on the impact angle, for a 10 mm thick plate subjected to projectile velocities of 800, 1000, and 1500 m/s. At 800 m/s, the projectile caused partial damage to the plate but did not perforate it. At 1000 m/s, partial damage occurred at an impact angle of 30°, while full perforation was observed at 0° and 15°. At 1500 m/s, the projectile penetrated the plate at all three impact angles.

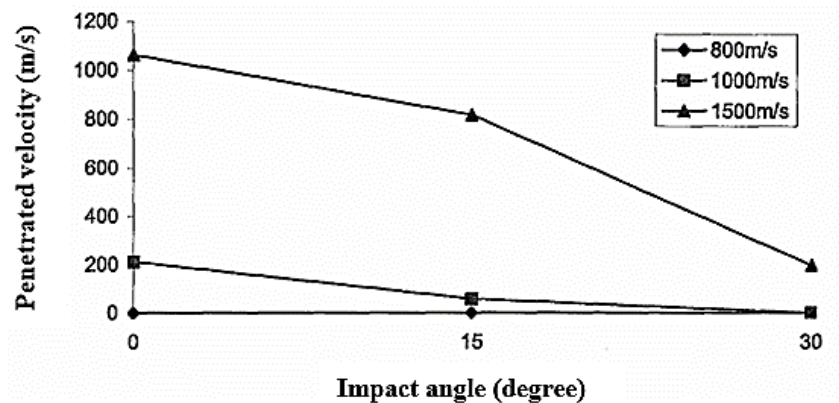


Figure 5. Relationship between penetrated velocity and impact angle for a 10 mm thick plate subjected to projectile velocities of 800, 1000, and 1500 m/s.

3.3. Validation of numerical simulations

ANSYS-based finite element analyses yielded results that were largely consistent with experimental data. In particular, post-impact deformation patterns, stress propagation, and structural responses were successfully represented through numerical modeling. The Johnson–Cook material model adequately described the behavior of materials under high-strain-rate deformation conditions [12]. However, in certain configurations, the elastomeric interlayer appeared stiffer than observed experimentally, indicating the need for a more detailed definition of viscoelastic material models.

3.4. Engineering perspective

According to the findings, not only material selection but also layer configuration, interlayer material type, and thickness distribution are critical in armor design [22]. The combined use of harder steels like MARS 240 with MARS 190 provided balanced performance in terms of both impact resistance and post-failure structural integrity. Especially, multilayered structures offer advantages not only in terms of mechanical strength but also in terms of protection-to-weight ratio [23]. In this respect, the study provides valuable insights for the development of lightweight, high-performance armor systems in the future.

4. Conclusions

This study investigated the ballistic performance of various armor configurations made from high-strength steels MARS 190 and MARS 240 through experimental testing and finite element simulations. Results demonstrate that material selection, layer configuration, and interlayer composition significantly influence impact resistance and structural response.

The main findings of the study are as follows:

- **MARS 240 steel**, due to its high hardness, demonstrated superior resistance to low- and medium-velocity impacts, but exhibited brittle behavior at higher impact velocities.
- **MARS 190 steel**, with its more ductile structure, maintained its integrity even under high levels of deformation.
- **Two-layer structures** were found to distribute impact energy more effectively than single plates, reducing rear-face deformation.
- The **steel–rubber–steel configuration** exhibited the highest energy absorption performance, attributed to the damping of stress waves by the elastomeric interlayer.
- The **steel–air gap–steel configuration** dissipated the initial impact energy within the first layer, significantly reducing the energy transmitted to the second layer—supporting the effectiveness of spaced armor systems.
- **Numerical analyses** showed strong agreement with experimental findings; the Johnson–Cook material model effectively represented high-velocity deformation behavior with sufficient accuracy.

These results indicate that in the design of armor systems, not only the material type but also the layer configuration, interlayer material combinations, and the configuration selection based on impact scenarios play a critical role. The combined or strategically layered use of MARS 190 and MARS 240 steels enables the development of optimized armor systems in terms of both ballistic performance and structural integrity.

Declaration of competing interest

The authors declare that they have no any known financial or non-financial competing interests in any material discussed in this paper.

Author contribution

The contribution to the paper is as follows: Osman İyibilgin was responsible for the study conception and design, as well as the analysis and interpretation of the results. Abdullah Mimaroglu contributed by preparing the initial draft of the manuscript. All authors reviewed and approved the final version of the manuscript.

References

- [1] O. G. Bilir, T. Başer, B. Barutçuoğlu, A. Bayram, M. Uzunboy, and E. Erişir, “Mechanical-Properties-Based Ballistic Performance Prediction of Candidate Armor Steels,” *J. Mater. Eng. Perform.*, vol. 32, no. 17, pp. 7640–7650, Sep. 2023, doi: 10.1007/s11665-023-08165-0.
- [2] C. Du, G. Yang, D. Hu, and C. Li, “Study of Ballistic Impact Performance of the Bioinspired Flexible Multilayered Filling Armor by Different Projectiles,” *J. Mater. Eng. Perform.*, 2025, doi: 10.1007/s11665-025-10698-5.
- [3] P. S. Patil and N. K. Naik, “Ballistic impact performance of spaced multilayered and monolithic composite targets: Analytical and experimental studies,” *Int. J. Damage Mech.*, vol. 27, no. 9, pp. 1352–1379, 2018, doi: 10.1177/1056789517732376.
- [4] O. İyibilgin, “Bilgisayar destekli yüksek hızlarda çarpma analizi,” Sakarya University, Institute of Natural Sciences, Sakarya, 2004.
- [5] L. Tilsley, D. J. Carr, C. Lankester, and C. Malbon, “Do air-gaps behind soft body armour affect protection?,” *J. R. Army Med. Corps*, vol. 164, no. 1, pp. 15–18, 2018, doi: 10.1136/jramc-2016-000759.
- [6] L. Peterson, M. Horstemeyer, T. Lacy, and R. Moser, “Using an Internal State Variable Model

- Framework to Investigate the Influence of Microstructure and Mechanical Properties on Ballistic Performance of Steel Alloys,” *Metals (Basel)*., vol. 13, no. 7, 2023, doi: 10.3390/met13071285.
- [7] N. Thakur, P. Kumar, and R. S. Bharj, “Effect of Variation of Johnson-Cook Parameters on Kinetic Energy and Simulation of 4340 Steel Projectile,” *Mater. Today Proc.*, vol. 5, no. 14, pp. 27884–27892, 2018, doi: 10.1016/j.matpr.2018.10.027.
- [8] T. Fräs, C. C. Roth, and D. Mohr, “Dynamic perforation of ultra-hard high-strength armor steel: Impact experiments and modeling,” *Int. J. Impact Eng.*, vol. 131, no. May, pp. 256–271, 2019, doi: 10.1016/j.ijimpeng.2019.05.008.
- [9] J. Octavian and L. Simona, “Ballistic performance of monolithic rubber-ceramic composite armor,” *J. Compos. Mater.*, vol. 58, no. 5, pp. 689–706, 2024, doi: 10.1177/00219983231226412.
- [10] R. F. P. Junio, B. S. A. de Cêa, D. S. Silva, É. P. L. Júnior, S. N. Monteiro, and L. F. C. Nascimento, “Computational and Experimental Ballistic Behavior of Epoxy Composites Reinforced with Carnauba Fibers: A Stand-Alone Target and Multilayered Armor System,” *Polymers (Basel)*., vol. 17, no. 4, pp. 1–37, 2025, doi: 10.3390/polym17040534.
- [11] S. Khare, K. Kumar, S. Choudhary, P. K. Singh, R. K. Verma, and P. Mahajan, “Material Characterization of Armor Steel and Investigation of Its Ballistic Performance,” *J. Mater. Eng. Perform.*, vol. 32, no. 15, pp. 6833–6849, 2023, doi: 10.1007/s11665-022-07590-x.
- [12] W. J. Johnson, G.R.; Cook, “A constitutive model and data for metals subjected to large strains, high strain rates and high temperatures,” *Eng. Fract. Mech.*, vol. 21, pp. 541–547, 1983.
- [13] Yılmazçoban I.K., İyibilgin O., Mimaroglu İ., Ünal H. “Modelling a medical wheelchair frame, subject to impact loading,” pp. 100–102, 2010.
- [14] C. Liu and Y. X. Zhang, “Modelling mechanical behavior of aluminium foam under compressive loading using representative volume element method,” *11th World Congr. Comput. Mech. WCCM 2014, 5th Eur. Conf. Comput. Mech. ECCM 2014 6th Eur. Conf. Comput. Fluid Dyn. ECFD 2014*, vol. 5, no. Wccm Xi, pp. 2909–2915, 2014.
- [15] D. S. Silva, R. F. P. Junio, M. H. P. da Silva, and S. N. Monteiro, “Ballistic Performance of Raffia Fiber Fabric Reinforcing Epoxy Composites as Standalone Targets,” *J. Compos. Sci.*, vol. 8, no. 9, 2024, doi: 10.3390/jcs8090370.
- [16] A. Mimaroglu, O. İyibilgin, and H. Unal, “Ballistic penetration into targets: Use of F.E.technique,” in *Proceedings of the IASTED International Conference on Modelling and Simulation*, Montreal, 2006. [Online]. Available: https://www.researchgate.net/publication/262253464_Ballistic_penetration_into_targets_Use_of_FEtchnique
- [17] X. Zhang *et al.*, “Determination of Johnson–Cook Constitutive of 15-5 PH Steel Processed by Selective Laser Melting,” *Materials (Basel)*., vol. 16, no. 2, 2023, doi: 10.3390/ma16020800.
- [18] X. Guo, G. Yang, G. J. Weng, and L. L. Zhu, “Numerical simulation of ballistic performance of bimodal nanostructured metals,” *Mater. Sci. Eng. A*, vol. 630, pp. 13–26, 2015, doi: 10.1016/j.msea.2015.01.081.
- [19] Y. Shi, C. Mao, Z. Yang, R. Chen, and C. Zhang, “Numerical study on damage behavior of sandwich panels with fiber metal laminates skins subjected to blast and high-velocity fragments impact,” *Mech. Adv. Mater. Struct.*, vol. 0, no. 0, pp. 1–17, 2025, doi: 10.1080/15376494.2025.2452370.
- [20] E. O. Kondryakov, V. E. Danylyuk, and V. V. Kharchenko, “Fracture Energy Characteristics of High-Strength Steels Penetrated with Armor-Piercing Strikers at Velocities Up to 1000 m/s,” *Strength Mater.*, vol. 55, no. 2, pp. 245–253, 2023, doi: 10.1007/s11223-023-00519-2.
- [21] P. Kędzierski, A. Morka, G. Sławiński, and T. Niezgoda, “Optimization of two-component armour,” *Bull. Polish Acad. Sci. Tech. Sci.*, vol. 63, no. 1, pp. 173–179, 2015, doi: 10.1515/bpasts-2015-0020.
- [22] A. Sharma, R. Mishra, S. Jain, S. S. Padhee, and P. K. Agnihotri, “Deformation behavior of single and multi-layered materials under impact loading,” *Thin-Walled Struct.*, vol. 126, no. December 2016, pp. 193–204, 2018, doi: 10.1016/j.tws.2017.08.021.

- [23] D. Mohotti, T. Ngo, S. N. Raman, and P. Mendis, “Analytical and numerical investigation of polyurea layered aluminium plates subjected to high velocity projectile impact,” *Mater. Des.*, vol. 82, pp. 1–17, 2015, doi: 10.1016/j.matdes.2015.05.036.